Preprint
UCRL-JC-140493

The Treatment of Traction-Free Boundary Condition in Three-Dimensional Dislocation Dynamics Using Generalized Image Stress Analysis

T. A. Khraishi, H. M. Zibib T. Diaz de la Rubia

This article was submitted to
Dislocations 2000, Gaithersburg, MD., June 19-22, 2000

September 20, 2000

U.S. Department of Energy
Lawrence
Livermore
National
Laboratory

DISCLAIMER

This work was performed under the auspices of the United States Department of Energy by the University of California, Lawrence Livermore National Laboratory under contract No. W-7405-Eng-48.

The Treatment of Traction-Free Boundary Condition in Three-dimensional Dislocation Dynamics using Generalized Image Stress Analysis

Tariq A. Khraishi [a], Hussein M. Zbib [a,*], Tomas Diaz de la Rubia [b]

[a] School of Mechanical and Materials Engineering, Washington State University, Pullman, WA 99164-2920, USA
[b] Chemistry and Materials Science, Lawrence Livermore National Laboratory, Livermore, CA 94550

Abstract

Recent attention has been given to the proper treatment of the planar traction-free surfaces which typically bound a computational box in three-dimensional dislocation dynamics. This paper presents an alternative to the use of the finite-element method for this purpose. Here, to annul the tractions produced by a sub-surface dislocation segment on a finite-area free surface **S**, a combination of an image dislocation segment, and a distribution of N prismatic rectangular Volterra dislocation loops meshing **S** is utilized. The image dislocation segment, with the proper sign selection of the Burgers vector components, annuls the shear stresses, and the normal stress component is annulled discretely at N collocation points representing the centers of the loops. The unknowns in this problem are the magnitudes of the N Burgers vectors for the loops. Once these are determined, one can back calculate the Peach-Koehler force acting on the sub-surface segment and representing the effect of the free surface. As expected, the accuracy of the method improves as the loops continuously decrease in size.

1. Introduction

Dislocation dynamics, or DD, has recently emerged as a powerful method for predicting the plastic deformation of defected crystalline materials [1, 2]. DD deals with the interaction of

* Corresponding author. Tel.:509-335-7832; fax:509-335-7832.
E-mail address: zbib@mme.wsu.edu (Hussein M. Zbib)

three-dimensional dislocation curves located in a simulation box (representing a single crystal) and approximated as a set of connected dislocation line segments each. The self-stress of a straight-line dislocation segment in an *infinite medium* can be found from the literature [3,4]. This self-stress represents the main ingredient in dislocation dynamics codes, needed in order to capture the mutual interaction of the segments.

When the dislocation segments are close to external free surfaces (e.g. the computational domain boundaries), the self-stress formula used previously is no longer valid by itself and should instead be augmented with auxiliary terms. Such terms arise, e.g., from image stresses when dealing with infinitely long dislocation lines near a free surface. These terms represent the effect of the free surface on the nearby dislocation segment. Thus, current implementations of dislocation dynamics are not completely accurate since they consider the dislocations to lie in an infinite medium. Instead, the effect of a finite domain, through the computational cell surfaces, needs to be examined.

The objective of this study thus is to rigorously treat the traction-free condition imposed on the boundaries of a DD box. The study provides for theoretical and numerical treatments of the condition. It is based on image stress analysis (from dislocation theory) and derives from crack theory. Its approach can be categorized under "generalized image stress analysis," which here refers to the careful distribution of dislocation entities (lines, loops, etc., that are sources of stress), at or near the boundary of interest such that the zero-traction condition is satisfied. The proper treatment of this boundary condition should improve the DD prediction of macroscopic material behavior, and eliminate any hidden or not readily apparent artifact or bias in the results.

With regard to the effect of free surfaces on sub-surface dislocations, several researchers have investigated different aspects of the problem. Initially, [5] determined the elastic fields of a

dislocation half-line terminating at a free surface of an isotropic elastic body for any angle of incidence and Burgers vector. The displacements of an infinitesimal dislocation loop of arbitrary orientation, and residing in a semi-infinite isotropic elastic medium, were obtained by [6]. The elastic field of a closed finite, or semi-infinite, dislocation loop can thus be obtained by means of area integration using the results for the infinitesimal loop. Using results from [6], [7,8] derived the stress fields of a dislocation half-line (and segment) parallel and perpendicular to a free surface of a semi-infinite isotropic medium. Concurrently with the works of [7,8], [9] found the displacement field associated with an angular dislocation in an elastic isotropic half space. For a dislocation half-line in an isotropic half-space, [10] have obtained closed form solutions for the stresses, which can be used to find the stresses of a line segment. Finally, [11] developed an integral expression for the case of a dislocation terminating at the free surface of an anisotropic half-space. They solved the problem using a planar fan-shaped distribution of infinite straight dislocations. This idea is similar to solving crack problems by the proper distribution of stress sources (i.e. dislocation entities).

2. Treatment of the Traction-Free Surface Problem

Consider Fig. 1 below showing a sub-surface dislocation segment A_1B_1. Here, **b** is the Burgers vector of the segment and $\mathbf{t}_1$ is its line sense. The condition of zero traction requires that $T = \sigma n = 0$ at any surface point, P, which translates to $\sigma_{xz} = \sigma_{yz} = \sigma_{zz} = 0$. To annul the shear stresses on the plane, one can place a mirror segment A_2B_2 such that $\boldsymbol{b}_z^{A_2B_2} = \boldsymbol{b}_z^{A_1B_1}, \boldsymbol{b}_x^{A_2B_2} = -\boldsymbol{b}_x^{A_1B_1}$, and $\boldsymbol{b}_y^{A_2B_2} = -\boldsymbol{b}_y^{A_1B_1}$. This can be proven after some careful analysis of the segments' stress fields (available in [3,4]). This image solution, however, does not annul the σ_{zz} component of stress. In fact the contributions of each segment at the surface points is equal and additive.

Consider area S in Fig. 1 on which the annulment of σ_{zz} is desired. This finite area represents a portion of the parent surface area. Let's further subdivide S into N rectangular surface elements representing prismatic dislocation loops with unknown Burgers vectors. One such loop, *Loop i*, is shown in Fig. 1, illustrating its line sense and Burgers vector with respect to a body-fixed coordinate system $x'y'z'$. The loop center, in global coordinates, is $(x^i_{o'}, y^i_{o'}, z^i_{o'})$. We propose to annul the σ_{zz} component in a discrete fashion by requiring it to be identically zero at the centers of these elements. This of course does not necessarily ensure its annulment at other surface points. Therefore this technique is numerical and approximate in nature. More accuracy can be attained by further subdividing S into an increasing number of elements, i.e. using smaller loops, which will cause the enforcement of the boundary condition at more collocation points (covering the whole surface in the limit).

The problem here thus reduces to finding the set of loops' Burgers vectors that will collectively satisfy the boundary condition at the collocation points. Once these are solved for, the Peach-Koehler force acting on the sub-surface segment will be due to externally applied stresses, the stress fields of the mirror reflected segment and the surface prismatic loops. The stress field of a prismatic loop can typically be derived from the Peach-Koehler equation. This equation expresses the stress field of an arbitrarily curved dislocation in terms of a line integral [3]. Indeed, we have obtained such a stress field as just suggested and exclude it here due to its length. The reason for picking loops of prismatic character is that these loops have a non-vanishing σ_{zz} component as well as null shear stresses in their plane. Note that the above-proposed method is in harmony with the idea of "generalized image stress analysis" discussed earlier.

Based on the above, the annulment of the σ_{zz} component of stress at the center of any loop, *i*, can be stated as:

$$\sigma_{zz}^{i} = -\sum_{\substack{j=1 \\ j\neq i}}^{N} \sigma_{zz}^{j} - \sigma_{zz}^{A_1B_1} - \sigma_{zz}^{A_2B_2} \qquad ,i = 1 \cdots N \qquad (1)$$

, where σ_{zz}^{j} is the stress from *Loop j*, and $\sigma_{zz}^{A_1B_1}$ is the stress from segment A_1B_1. Note that the unknown in each of the loop stress terms in (1) is the magnitude of the prismatic Burgers vector (b_z) of that loop. In each of these terms b_z pre-multiplies another term or kernel *K(x,y)*. Hence, for each collocation point *i*, Eq. (1) corresponds to a linear relation between N unknown loop b_z magnitudes. Applying (1) N times at the centers of all loops produces a set on N linear algebraic equations with N unknowns to solve for.

Note that the above devised numerical scheme is self-consistent geometrically, numerically, and within the context of dislocation theory. Note also that the extent of area **S** upon which the boundary condition is enforced is a problem parameter and can be extended almost indefinitely. Finally, note that the choice of dislocation loops to annul any undesirable surface tractions is advantageous because the stress field of such loops decays rapidly as $1/r^3$. Therefore, the loop distribution on one free surface, say corresponding to one of the boundaries of a finite cubic computational cell, will have little effect on the tractions on other nearby perpendicularly oriented surfaces. Therefore, an assumption of uncoupling in the image treatment of the different surface will not be far fetched here.

Consider Eq. (1) again. It can be rewritten as:

$$\sum_{j=1}^{N} \sigma_{zz}^{j} = -\sigma_{zz}^{A_1B_1} - \sigma_{zz}^{A_2B_2} = -2\sigma_{zz}^{A_1B_1} \qquad ,i = 1 \cdots N \qquad (2)$$

, knowing that the contributions of segments A_1B_1 and A_2B_2 are equal. Now, recognizing that

$\sigma_{zz}^{A_1B_1}$ evaluated in the S plane is a function of x and y only, (2) can be written:

$$\sum_{j=1}^{N} b_z^j K(x_O^i - x_O^j, y_O^i - y_O^j) = -2\,\sigma_{zz}^{A_1B_1}\Big|_{center\ of\ Loop\ i} = -f(x_O^i, y_O^i) \qquad i = 1\cdots N, \quad (3)$$

The σ_{zz} component of a square prismatic loop of half-side a centered at the origin of the xyz system and evaluated in the loop plane (i.e. z=0) simplifies to:

$$\sigma_{zz} = b_z K(x,y) = \frac{G b_z}{4\pi(1-\nu)} \left(\begin{array}{l} \dfrac{\sqrt{(a-x)^2+(a-y)^2}}{(a-x)(a-y)} + \dfrac{\sqrt{(a+x)^2+(a-y)^2}}{(a+x)(a-y)} \\ + \dfrac{\sqrt{(a-x)^2+(a+y)^2}}{(a-x)(a+y)} + \dfrac{\sqrt{(a+x)^2+(a+y)^2}}{(a+x)(a+y)} \end{array} \right) \qquad (4)$$

Here, $K(x,y)$ is the sought after kernel in Eq. (3) above.

From (3) above, one can see that we have an N_N system of linear algebraic equations:

$$\underbrace{[A]}_{N\times N}\ \underbrace{\{b_z\}}_{N\times 1} = \underbrace{\{C\}}_{N\times 1} \qquad (5)$$

, where the $[A]$ matrix contains interacting kernels and $\{C\}$ is like a forcing vector containing the negatives of $f(x,y)$. This system can be solved using the solver of choice.

Results and Discussion

Once the Burgers vectors of the surface loops are known, one can compute the Peach-Koehler force (PKF) on a sub-surface segment. The PKF acting on the segment tends to pull it towards the surface to minimize the crystal energy. Due to elasticity theory limits, the force on a segment can only be calculated to within a core distance or depth (i.e. z-depth = 0.5b-4b) from the surface. This is not a serious limitation and is in harmony with other DD calculations which take this limitation into account and deal with it similarly.

Comparisons between our solution for a horizontal sub-surface segment have been made with the solution of [7] for a half-plane. At the outset, one needs to recognize that the two solutions

will not match due to area size differences. However, if one chooses a large enough area, and a small enough segment away from the area corners and close to the finite plane, one should expects a good resemblance between the two solutions. In all of the results below, the segment length is equal to $100b$ (where b is the magnitude of the crystal's Burgers vector), the shear modulus is 42.25GPa and the Poisson ratio is 0.383.

Consider a horizontal segment, A_1B_1, at a depth of $1000b$, lying parallel to the x-axis, and having a normalized Burgers vector $\mathbf{b}=(1/\sqrt{3},1/\sqrt{3},1/\sqrt{3})$. The coordinates of A_1 and B_1 are $(100b,0,-1000b)$ and $(0,0,-1000b)$, respectively. The finite surface area represents a rectangle with a side of $20{,}000b$. If one compares the σ_{xx}, σ_{yy}, and σ_{zz} components using the above method with the method of [7], one gets Figs. 2 and 3. In these plots the evaluation points are chosen to lie at a depth of $400b$ parallel to the x-axis with $y = 0$. In Fig. 2, the finite area was divided into 30◈30 intervals totaling 900 loops. The surface loop density is increased in Fig. 3 to 50◈50 (2500 loops)

In Fig. 2, the stresses obtained by the two methods follow similar trends but noticeably differ in value, perhaps due to the low loop density used in conjunction with the current solution. As the loop density increases to 50◈50 (Fig. 3), the two methods give almost identical results, at least for the σ_{xx} and σ_{zz} components. Increasing the meshing density further will enhance the agreement between the σ_{xx} and σ_{zz} components and stabilize (the noted) difference in the σ_{yy} results. This difference is due to the different area sizes utilized in each of the methods, and the current solution will converge towards the half-plane solution as the conditions of the problem resemble more that of a half-plane problem. This can be attained for example if the dislocation segment gets closer to the surface while staying away from the edges of S. If one now instead

plots the variation σ_{xy}, σ_{xz}, and σ_{yz} in the x-direction, one would also get good agreement between the current solution and [7].

At a meshing density of 50x50 loops (Fig. 3), the average separation distance between the surface collocation points is roughly 400b. Incidentally, this is the same sub-surface depth chosen for the evaluation points in the figure. The reason for this coincidence can be explained by St. Venant's Principle in elasticity theory, which states that agreement between an exact solution and an approximate, but functionally equivalent, one at a boundary will be good for field points lying more than a "characteristic" distance away from the boundary. The characteristic distance in this case being the average separation distance between collocation points at which the boundary condition is enforced.

Finally, some results from incorporating the above method into our DD code are exhibited. Here all six faces of the cubic cell are padded with rectangular surface loops and an interior segment is reflected off of all these surfaces. The PKF on the segment is the sum of the forces from all six faces. Fig. 4 shows stress-strain diagrams obtained from DD simulations for a cubic specimen 10,000b in size subjected to a shearing load at a rate of 10 sec^{-1}. The solid curve represents a case of no surface loops and the dashed line represents 40◈40 surface loops meshing. One can see that the surface effect acts to lower the saturation stress level in the stress-strain diagram. Here the source is initially away from the walls. As the Frank-Read source starts to emit dislocation loops or lines, they come into proximity with the surfaces at some point. Once the dislocation lines (or segments) are close to an exterior wall, an attraction force, pulling them towards the surface, further assists their glide. This force comes from the image stress analysis, i.e. from the proper treatment of the traction-free boundary condition.

Before ending it is important to note that a surface-piercing segment represents a special case of a sub-surface segment and hence can be treated using the above method, as long as the piercing point lies within a surface loop not touching a loop's edge.

Acknowledgements

This work was performed in part under the auspices of the US Department of Energy by University of California Lawrence Livermore National Laboratory under contract W-7405-Eng-48. The support of Lawrence Livermore National Laboratory to WSU is gratefully acknowledged.

References

[1] H. M. Zbib, M. Rhee, J. P. Hirth, Int. J. Mech. Sci. 40 (1998) 113.

[2] M. Rhee, H. M. Zbib, J. P. Hirth, H. Huang, T. D. de la Rubia, Modelling Simul. Mater. Sci. Eng. 6 (1998) 467.

[3] J. P. Hirth, J. Lothe, Theory of Dislocations, Krieger Publishing Company, Malabar, Florida, 1982.

[4] B. Devincre, Solid State Communications 93 (1995) 875.

[5] E. Yoffe, Philosophical Magazine 6 (1961) 1147.

[6] P. P. Groves, D. J. Bacon, Philosophical Magazine 22 (1970) 83.

[7] Y. Maurissen, L. Capella, Philosophical Magazine 29 (1974) 1227.

[8] Y. Maurissen, L. Capella, Philosophical Magazine 30 (1974) 679.

[9] M. Comninou, J. Dunders, J. Elasticity 5 (1975) 203.

[10] T. J. Gosling, J. R. Willis, J. Mech. Phys. Solids 42 (1994) 1199.

[11] J. Lothe, V. L. Indenbom, V. A. Chamrov, Phys. Stat. Sol. B111 (1982) 671.

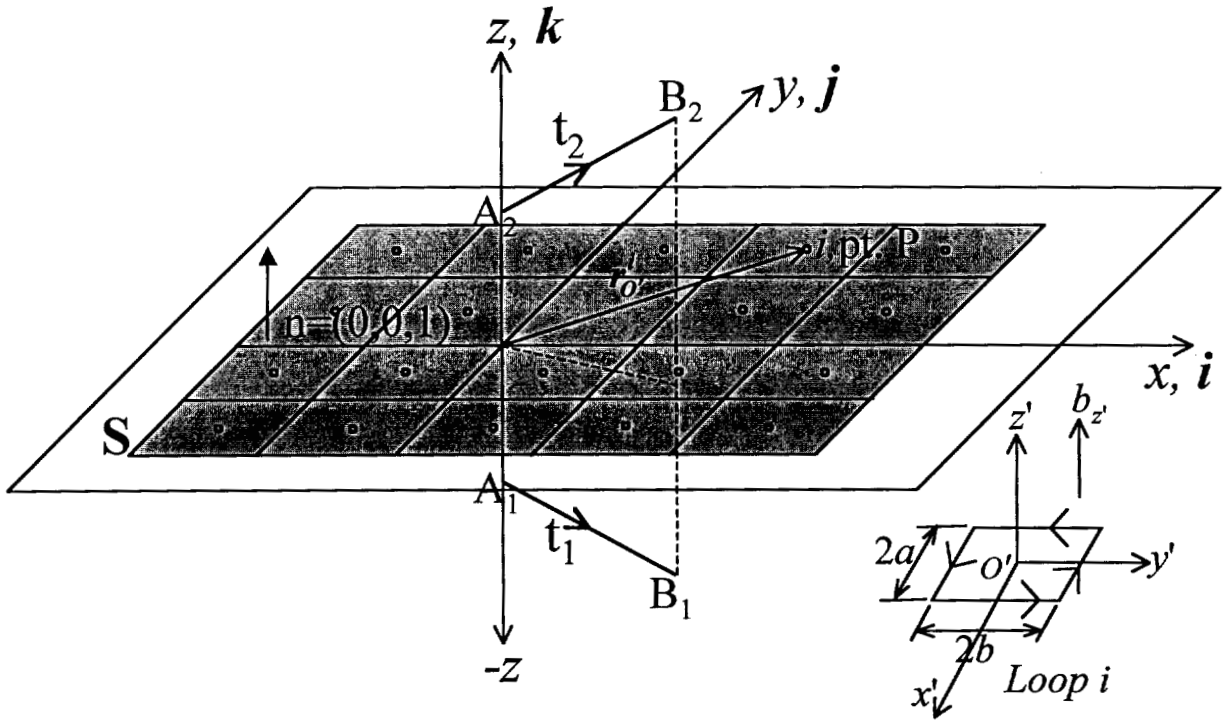

Fig. 1 A schematic of sub-surface segment A_1B_1 and its reflected image segment A_2B_2. Surface area **S** is divided into N rectangular elements representing prismatic dislocation loops (see inset). The traction-free boundary condition is imposed at the centers of the loops.

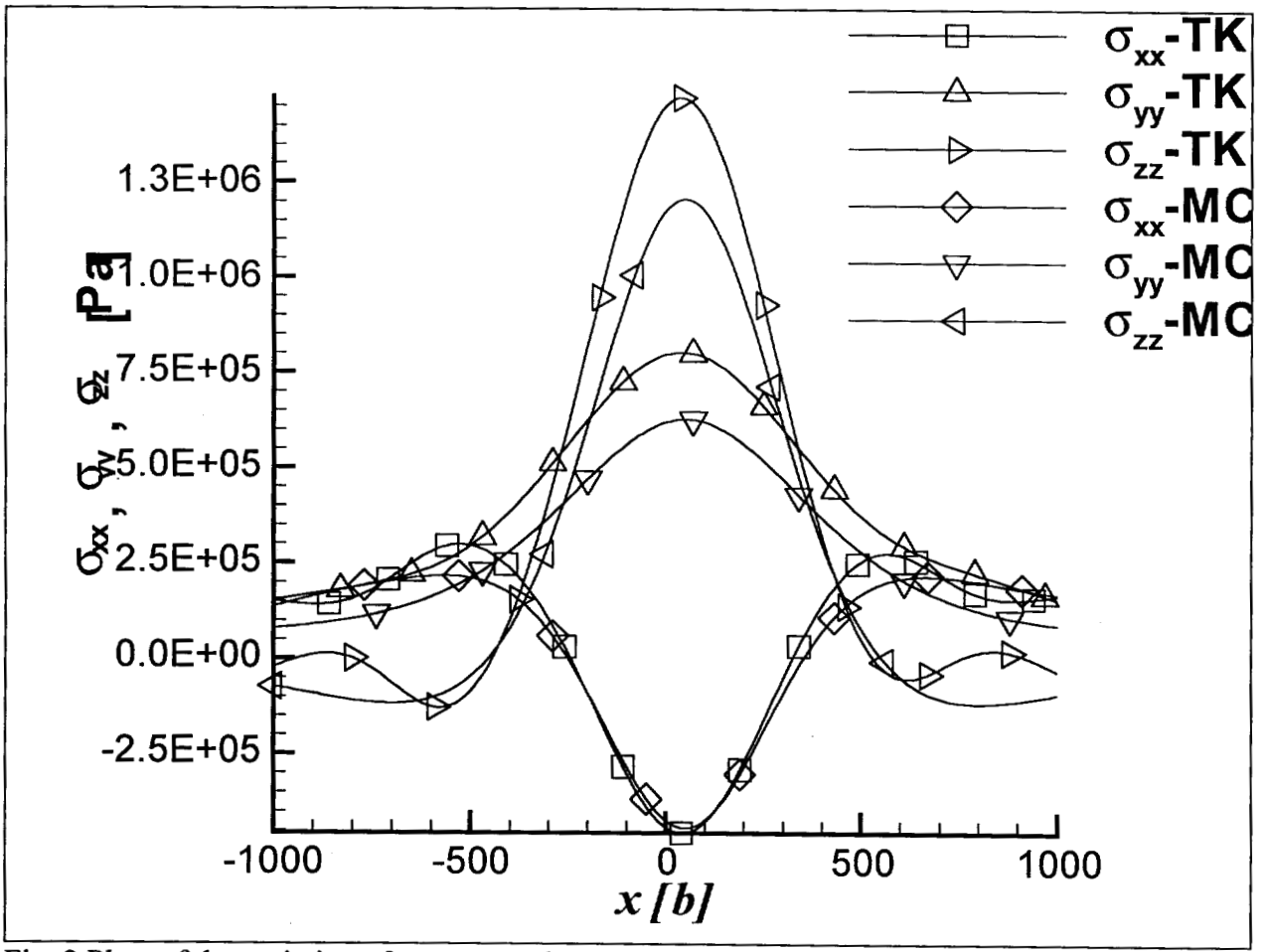

Fig. 2 Plots of the variation of σ_{xx}, σ_{yy}, and σ_{zz} versus x at a depth of $400b$ and for y=0. TK and MC indicate the current solution and the solution of [7], respectively. Here area S is square of size $20{,}000b$ and is divided into 30◈30 loops. The sub-surface segment is horizontal, $100b$ in length, at a depth of $1000b$, and has three non-zero components of Burgers vector.

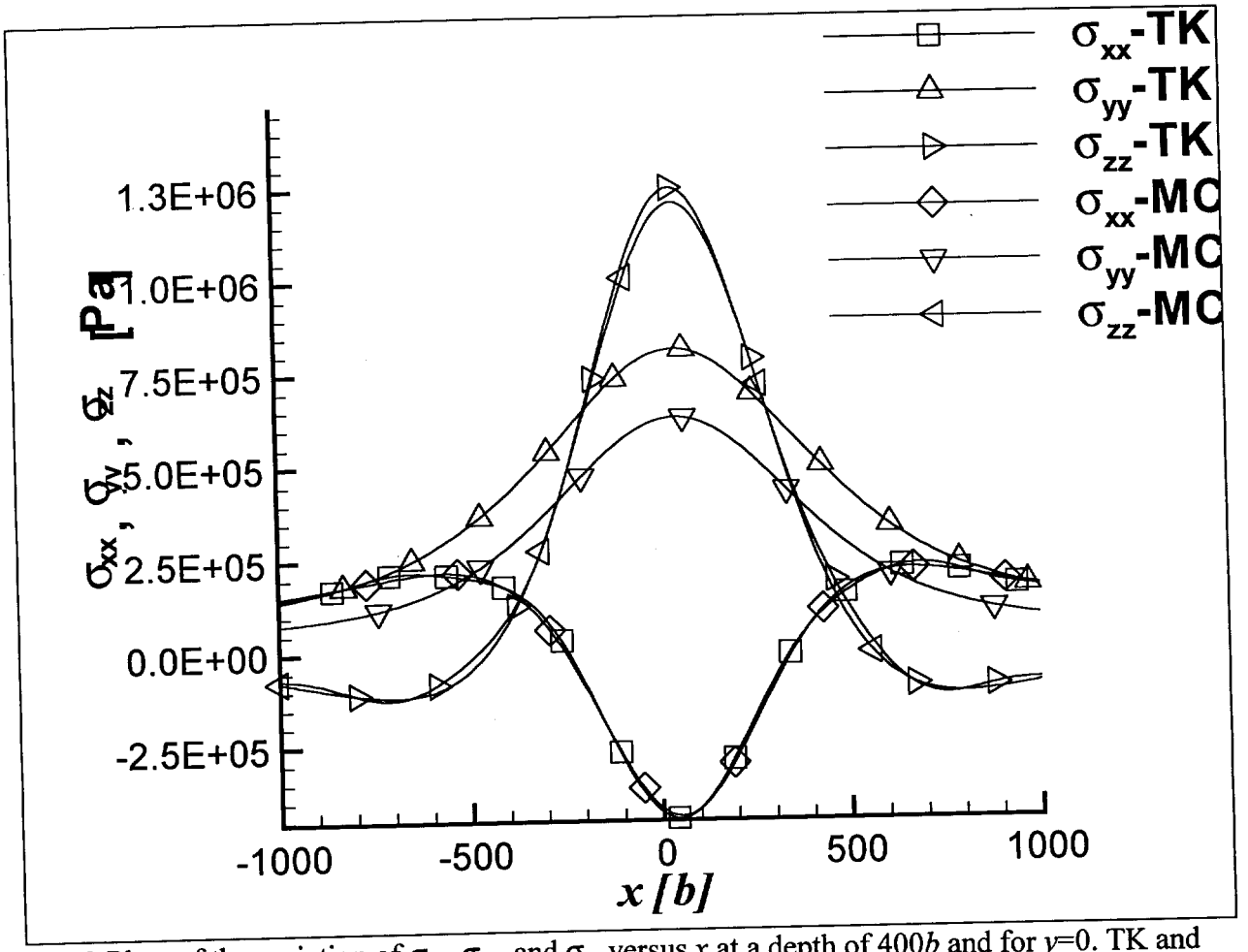

Fig. 3 Plots of the variation of σ_{xx}, σ_{yy}, and σ_{zz} versus x at a depth of $400b$ and for y=0. TK and MC indicate the current solution and the solution of [7], respectively. Here area S is square of size $20{,}000b$ and is divided into 50◈50 loops. The sub-surface segment is horizontal, $100b$ in length, at a depth of $1000b$, and has three non-zero components of Burgers vector.

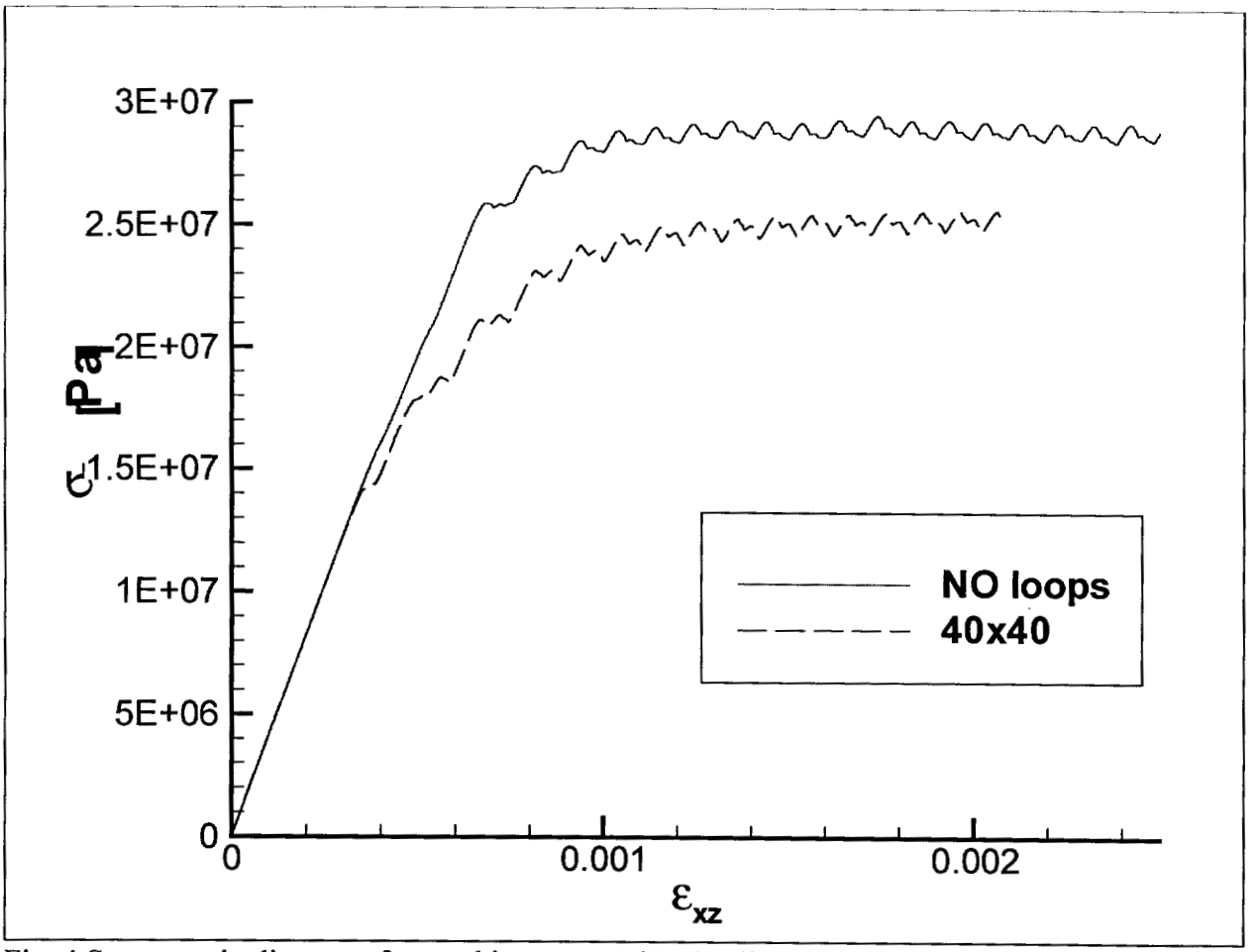

Fig. 4 Stress-strain diagrams for a cubic computational cell of 10,000*b* in size subjected to a shearing rate of 10 sec^{-1}. The solid curve represents a case of no surface loops (i.e. no treatment of the traction-free boundary condition) and the dashed line represents 40◈40 surface loops meshing.